

Size homeostasis in adherent cells studied by synthetic phase microscopy

Yongjin Sung^{a,1}, Amit Tzur^{b,c,1}, Seungeun Oh^b, Wonshik Choi^d, Victor Li^b, Ramachandra R. Dasari^a, Zahid Yaqoob^a, and Marc W. Kirschner^{b,2}

^aG. R. Harrison Spectroscopy Laboratory, Massachusetts Institute of Technology, Cambridge, MA 02139; ^bDepartment of Systems Biology, Harvard Medical School, Boston, MA 02115; ^cThe Mina and Everard Goodman Faculty of Life Sciences and the Institute for Nanotechnology and Advanced Materials, Bar-Ilan University, Ramat-Gan 52900, Israel; and ^dDepartment of Physics, Korea University, Seoul 136-701, Republic of Korea

Contributed by Marc W. Kirschner, August 29, 2013 (sent for review September 14, 2011)

The coupling of the rate of cell growth to the rate of cell division determines cell size, a defining characteristic that is central to cell function and, ultimately, to tissue architecture. The physiology of size homeostasis has fascinated generations of biologists, but the mechanism, challenged by experimental limitations, remains largely unknown. In this paper, we propose a unique optical method that can measure the dry mass of thick live cells as accurately as that for thin cells with high computational efficiency. With this technique, we quantify, with unprecedented accuracy, the asymmetry of division in lymphoblasts and epithelial cells. We can then use the Collins–Richmond model of conservation to compute the relationship between growth rate and cell mass. In attached epithelial cells, we find that due to the asymmetry in cell division and size-dependent growth rate, there is active regulation of cell size. Thus, like nonadherent cells, size homeostasis requires feedback control.

cell division asymmetry | cell growth | cell dry mass | interferometry | synthetic phase microscopy

Size is an important phenotypic characteristic of any cell with consequences for tissue and organ architecture. The process by which cells regulate their size has fascinated generations of biologists, but the details have remained largely obscure, largely because accurate measurements at the single-cell level were difficult to carry out (1). In proliferating cells, size is the result of cell growth (which steadily increases the cell's size) and cell division (which roughly halves the cell size each generation). Cells proliferating in constant conditions maintain a particular size distribution, suggesting that these two processes are coordinated (2). In yeast, there is evidence for intrinsic “size-sensing” mechanisms that coordinate their size-dependent (exponential) growth with division in a way that limits size variation (e.g., refs. 3, 4). In metazoan cells, separate growth and mitogenic signals from the environment can independently regulate cell growth and division, and eventually cell size, in some circumstances, perhaps implying that cell-autonomous mechanisms linking cell growth with the division cycle may not exist in animal cells (5). This notion is further supported by the fact that early embryonic cell divisions are decoupled from cell growth. The increase in cell number is balanced by the decrease in cell size so that the embryo size remains constant. This classic debate has been revived recently, with strong evidence both for linear (size-independent) growth kinetics in primary Schwann cells (5, 6) and for size-dependent growth in lymphoblast, osteoblast, and adenocarcinoma cells (7–10). In the case of lymphoblasts, the division of volume among daughter cells has also been observed to be uneven. This implies that these cells at least actively coordinate cell growth with division to maintain a consistent size distribution in the population (10). The varying evidence on growth coordination may result from the different methodologies used, but it also may suggest that different types of animal cells have fundamental differences with regard to how they grow and maintain their size. It has been challenging to resolve this issue due to the serious difficulty in determining the exact size of cells, particularly when they are asymmetrical or

irregularly shaped, which, in turn, makes it difficult to derive the growth kinetics of living cells and their size variation upon division.

There is a confusion about what we should mean by “size” in the context of growth. For most measurements, size refers to geometric size or cell volume. Light microscopy and impedance-based tools (Coulter principle) have long been used for volume measurements. Microscopy is, by nature, a single-cell measurement; however, calculating volume is not straightforward in irregularly shaped cells. Impedance measurement is relatively insensitive to shape but, typically, can only be used for cell populations in suspension (11). Several surrogates for size have been used in the context of growth studies, including total (ribosomal) RNA and protein level or synthesis rate (e.g., refs. 12–14), the mRNA level for constitutively expressed genes (e.g., ref. 15), and the rate of uptake of nutrients/metabolites (e.g., ref. 16). It is simplest to consider growth as the creation of new biomass, mainly proteins, carbohydrates, and lipids. Cell mass is proportional to the volume if cell density remains constant, which seems true for some cells [e.g., murine lymphoblasts (17)] but not for others (18). Emerging technologies to weigh the mass (9) or the buoyant mass (18) of cells over time have been developed and used for cell size and growth studies. Some of these have very high precision (7) but are presently limited to unattached cells, and therefore have been used primarily for cells of hematopoietic origin. In contrast, optical methods are suitable for measuring the dry mass (mass of nonaqueous content) of adherent cells with high accuracy and minimal perturbation. In the simplest approach (8, 19), the retardation of light traversing the cell is related to the cumulative refractive index of the cellular constituents along the optical axis. The validity of this “projection” approach, however, is questionable for thick specimens, such as mitotic and other spherical cells. This is because the light

Significance

Accurate measurement of cell size is critical in studies of cell growth. Optical methods based on interferometry are known to be suitable for attached cells, but the existing techniques were originally designed for thin samples and are not ideal for thick ones, such as mitotic cells. Synthetic phase microscopy (SPM), a new tomographic interferometric method, offers an elegant solution to this problem. This paper demonstrates the ability of SPM to measure the growth of mammalian cells accurately, and it demonstrates a clear requirement for feedback in the growth process.

Author contributions: Y.S., A.T., R.R.D., and M.W.K. designed research; Y.S., A.T., and S.O. performed research; Y.S., A.T., S.O., W.C., V.L., and M.W.K. analyzed data; and Y.S., A.T., S.O., W.C., Z.Y., and M.W.K. wrote the paper.

The authors declare no conflict of interest.

¹Y.S. and A.T. contributed equally to this work.

²To whom correspondence should be addressed. E-mail: marc@hms.harvard.edu.

This article contains supporting information online at www.pnas.org/lookup/suppl/doi:10.1073/pnas.1315290110/-DCSupplemental.

incident onto a cell is diffracted from the cell boundary and cell's internal organelles, and thus propagates within the sample like the ripples in water rather than a straight ray. Thus, the scalar diffraction theory may be more appropriate for interpreting the scattered light field from biological samples (20).

Here, we report a rigorous treatment of the light scattering by heterogeneous 3D structures in a cell to measure the dry mass in living cells accurately, regardless of their shape or optical depth. Our method measures the dry mass of thick samples as accurately as for thin samples; therefore, we can use it to study both size variation upon division and the growth kinetics of living cells. Specifically, we measure the dry mass of daughter cells immediately after division in L1210 lymphoblastoid cells and two epithelial cell types, HT-29 and RKO human colon cancer cells. We also measure the mass distribution of these cells growing naturally in constant conditions. Then, using the Collins–Richmond conservation principle (21), we obtain the relationship between growth rate and cell mass. Our findings of the asymmetry of cell division and the mass dependence of growth in epithelial cells demand an intrinsic mechanism for growth control like that proposed for bacteria (22), yeast (3, 4) erythroblasts (23), and lymphoblasts (7, 10).

Results

Synthetic Phase Microscopy for Dry Mass Measurement. The light field scattered from a sample carries the information about the sample in the form of amplitude modulation, wavefront distortion, or both. The wavefront modulation or phase delay, which can simply be related to the sample's refractive index in the visible regime, can be measured by Shack–Hartmann sensors (24, 25), interferometry (26–29), or propagation-based methods (30, 31). The linear relationship between the refractive index and the concentration of organic molecules is established well (32–35). Notably, for most of a cell's chemical components, the specific refraction increment α relating the refractive index and mass concentration remains constant regardless of the chemical identity of the biomaterial (35). For instance, the mean proportionality coefficient for the entire set of human proteins is 0.190 mL/g, with an SD of only 0.003 mL/g (35).

The scalar diffraction theory predicts that the scattered field for a specific angle of illumination onto an object provides a portion of the object spectrum in 3D spatial frequency space (36). Importantly, the information needed to calculate the dry mass of a specimen is mostly contained in the $W = 0$ plane (*SI Materials and Methods*), where W is the spatial frequency coordinate corresponding to the optical axis Z (Fig. 1A). Under the Rytov approximation (37), which is valid for most biological samples, the following relationship holds in the Fourier plane between the areal dry mass density $\sigma(X, Y)$ and the sample-induced phase delay $\Phi_{\vec{k}_0}(X, Y)$ recorded for a specific illumination angle (*SI Materials and Methods*):

$$\tilde{\sigma}(U, V) = \begin{cases} \frac{\lambda^2 w}{2\pi n_0 \alpha} \tilde{\Phi}_{\vec{k}_0}(U, V), & (U, V) \in C, \\ 0, & \text{otherwise,} \end{cases} \quad [1]$$

where $\tilde{\sigma}(U, V)$ and $\tilde{\Phi}_{\vec{k}_0}(U, V)$ are the 2D Fourier transforms of $\sigma(X, Y)$ and $\Phi_{\vec{k}_0}(X, Y)$, respectively. The subscript \vec{k}_0 indicates the direction of the incident beam: $\vec{k}_0 = (u_0, v_0, w_0)$. The set C is a collection of points (U, V) satisfying the following relationship: $(U+u_0)^2 + (V+v_0)^2 = (n_0/\lambda)^2 - w_0^2$. The refractive index of the background medium is n_0 , and λ is the wavelength of the incident light. By varying the angle of illumination (Fig. 1B), different portions of $\tilde{\sigma}$ can be obtained using Eq. 1 (Fig. 1C). Consequently, the areal density $\sigma(X, Y)$ of dry mass can be obtained by taking the inverse Fourier transform of $\tilde{\sigma}(U, V)$:

$$\sigma(X, Y) = \iint_{\Omega} \tilde{\sigma}(U, V) e^{j2\pi(UX+VY)} dU dV, \quad [2]$$

where Ω is the spatial frequency support determined by the N.A. of a synthetic phase microscopy (SPM) system. We note that the areal density image obtained with SPM (Fig. 1D) is free from the diffraction artifact that will be described more extensively below. In addition, the areal density in Eq. 2 is equivalent to the numerical projection of the 3D refractive index map obtained with optical diffraction tomography (ODT) (38). Therefore, SPM provides transverse resolution similar to that obtained with ODT, which is double the resolution available from single-shot phase imaging. We note that the computational efficiency is much higher in SPM, because it maps the measured scattered fields onto a 2D plane rather than a 3D spatial frequency space as in ODT. Fig. 1D compares areal density images of an RKO human colon cancer cell obtained with SPM and single-shot phase imaging. It is clear that the noise level in SPM is significantly lower than in single-shot phase imaging. For example, the dry mass value within the dotted region in the SPM image amounts to only 2.5 fg, which is comparable to the measurement noise of 6 fg in a suspended microchannel resonator (7). The high measurement sensitivity of SPM is attributed to significantly reduced coherent speckles, as in partially coherent imaging (39). To test the measurement accuracy of SPM, we quantified the refractive index of polystyrene beads and compared it with the value measured using a refractometer for bulk material (40). Note that we obtained the 2D phase images with SPM and calculated the refractive index of the beads using the spherical shape of the beads. The mean refractive index for the 20- μ m polystyrene beads ($n = 44$) was measured to be 1.5857 with an SD of 2×10^{-4} . This value matches very well with the refractive index of bulk polystyrene, which is 1.5872 at 633 nm.

Fig. 2A shows how the diffraction from small organelles can affect measured phase, and thus dry mass value. Phase images (i) and (ii) were obtained with single-shot phase imaging, whereas phase images (iii) and (iv) were acquired with the SPM method, and thus are diffraction-corrected. The objective focus was placed at the center of the bead for phase images (i) and (iii), and at 2 μ m above the center for phase images (ii) and (iv). If the projection assumption were valid or its error negligible, phase images (i) and (ii) should have shown a similar phase delay pattern even though they are taken at different heights; this is clearly not the case. This observation is consistent with our previous result that out-of-focus features are blurred and generate diffraction artifacts when the projection approach is adopted in tomographic reconstruction (38). The cell has a multitude of organelles, such as the nucleolus, mitochondria, and lipid droplets, and the objective focus is usually fixed at a location minimizing the diffraction pattern from the cell boundary. Therefore, out-of-focus organelles will introduce artifacts in a manner similar to the out-of-focus polystyrene bead in phase image (ii). On the other hand, SPM can correct this artifact; the phase delay patterns in phase images (iii) and (iv) are quite similar, although not exactly the same, perhaps due to the Brownian motion of the bead during data acquisition. Next, we tested the robustness of SPM for measuring cells of different shapes and optical thicknesses. We grew RKO cells on a poly-L-lysine-coated coverslip for 48 h, removed the slide from the incubator, and washed the cells with PBS. Using an on-stage flow chamber with an embedded heater, we observed the change in the measurement of cells' dry mass after adding trypsin. Within 10 min, the three cells in the middle of Fig. 2B changed their shape and their optical thickness at the center increased about 60%. However, the change in the dry mass measurement of the cells was less than 1% (SD) of the initial measurement. This shows that SPM measurements are almost entirely insensitive to cell thickness. In SPM, the cell dry mass is calculated by integrating

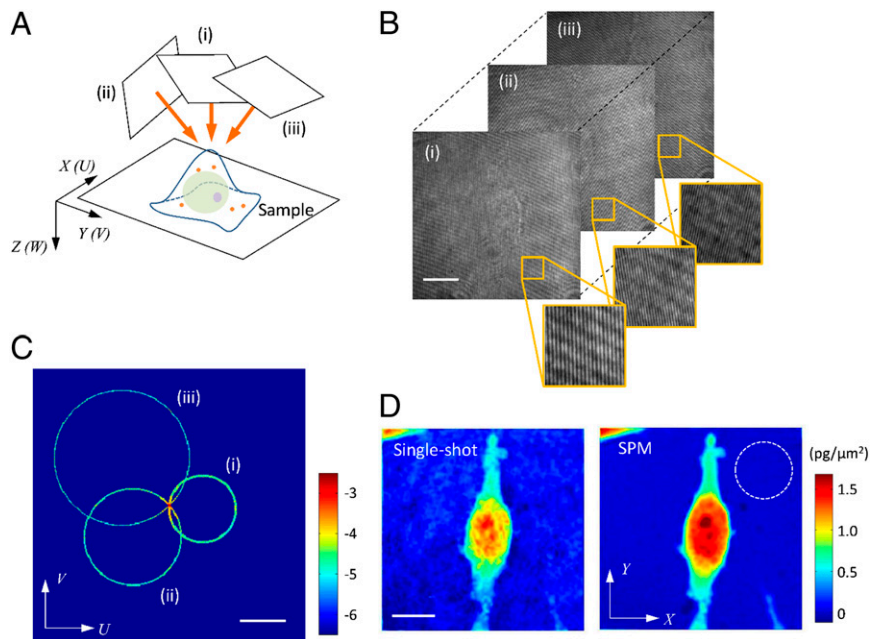


Fig. 1. SPM for dry mass measurements. (A) Spatial coordinates (X , Y , Z) and their associated spatial frequency coordinates (U , V , W) used in this paper are described. (B) Examples of raw interferogram images recorded at varying illumination angles: (i), (ii), and (iii). Each interferogram image provides both the amplitude and phase image of the scattered field from the sample at a specific illumination angle. (Scale bar, $10\ \mu\text{m}$.) (C) 2D mapping of the phase images in the spatial frequency plane using Eq. 1. The amplitude is shown in the logarithmic scale of base 10. (Scale bar, $1\ \mu\text{m}^{-1}$.) (D) Phase image for an RKO cell by single-shot phase imaging and synthesized using SPM. Dry mass averaged over the dotted line is the noise level of the measurement, which is $2.5\ \text{fg}$. (Scale bar, $10\ \mu\text{m}$.)

the measured areal density over the cell area. To determine the cell area, we use thresholding, which identifies the cells in the culture medium, together with manual selection, to separate one cell from another. Using two threshold levels (0.1 and $0.2\ \text{pg}/\mu\text{m}^2$) and repeating the selection of cell boundary three times, we estimated the uncertainty of SPM mass measurement due to boundary selection at less than $1\ \text{pg}$ in cells of an average mass of $348\ \text{pg}$, that is 0.3% ($n = 18$).

Cell Division Symmetry and Size Dependency of Growth Rate. Careful analysis of nearly spherical L1210 lymphoblasts revealed up to 7% differences in volume among daughter cells (10), emphasizing the need for a mechanism that regulates size homeostasis in these cells. However, optical measurements of adherent cells revealed volume changes in mitosis unrelated to biomass changes (41, 42), suggesting that cell size may not be accurately represented by volume at that stage. Therefore, it is not known to what extent biomass division is asymmetrical in animal cells, particularly for adherent amorphous cells. Dividing cells become round but not necessarily spherical, especially in adherent cell types. The asphericity (10), loss of contact area (9), or inadequacy of the projection assumption (19) hampers the application of other techniques for direct measurement of mitotic cell mass. We therefore first measured the daughter cell mass ratio for L1210 cells and found a division asymmetry of $7.5 \pm 4.8\%$ in dry mass (Fig. 3B, red), recapitulating the daughter cell size differences previously measured by volume (10). We thought that adherent cells, which interact with the surface and surrounding cells, might divide less evenly compared with the cells dividing in suspension. Indeed, the division asymmetry for both HT-29 (Fig. 3B, blue, $10.0 \pm 6.4\%$) and RKO (Fig. 3B, green, $13.0 \pm 6.8\%$) cells was significantly greater than for L1210 cells.

Cells proliferating in an unchanged environment (steady-state population) maintain a time-invariant cell size distribution (i.e., although cell number increases with time, the probability density of the cell size distribution remains constant at any time). If the

growth of cells is independent of their size, they could maintain the time-invariant size distribution independent of size checkpoint even if division is asymmetrical. By applying the Collins–Richmond model (21) to lymphoblastoid cell lines, Tzur et al. (10) showed a size-dependent growth rate and exponential growth pattern for these cells. Using our newly developed measurements, this analysis can now be improved. With respect to cell growth, mass is clearly a more relevant metric than volume. Moreover, this model for measuring growth patterns in adherent cells previously relied on assumptions with unknown validity (43). In this model, the growth rate of cells is calculated from three probability density functions for the asynchronous or steady-state populations, newly divided cells (newborns), and mitotic cells:

$$v(m) = \gamma \left(2 \int_0^m \phi(m') dm' - \int_0^m \theta(m') dm' - \int_0^m \chi(m') dm' \right) / \chi(m), \quad [3]$$

in which the functions $\phi(m)$, $\theta(m)$ are the probability densities in the size of newly divided cells (newborns) and mitotic cell populations, respectively, which, together, constitute the flux of division. The function $\chi(m)$ is the probability density in the size of asynchronous cells. The parameter γ is the division rate, representing the rate of increase in population (cell number) with time [more details and derivation are provided in refs. 10, 21].

Fig. 4A–C shows the calculated result for the Collins–Richmond model applied to L1210 lymphoblasts, which are round and only slightly adherent (Fig. 4A), and two adenocarcinoma cells of epithelial origin from the colon, HT-29 (Fig. 4B) and RKO (Fig. 4C), which are asymmetrical and strongly adherent. The inputs for the model (Fig. S1) were calculated by kernel density estimation, a nonparametric way of estimating the probability density based on a finite dataset (44, 45). The thick lines in Fig. 4A–C show the average growth rate, and the colored

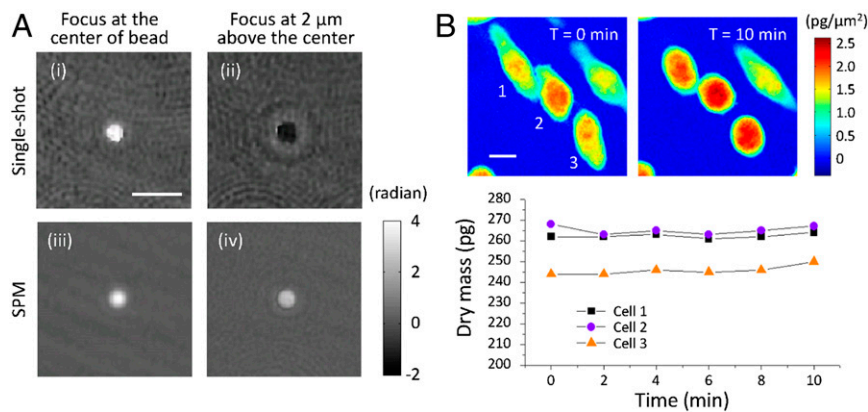


Fig. 2. (A) Bead defocus test with a 1- μm polystyrene bead immersed in water: focus at the center (*i* and *iii*), focus at 2 μm above the center (*ii* and *iv*), single-shot phase image (*i* and *ii*), and diffraction-corrected phase image by the SPM method (*iii* and *iv*). (Scale bar, 10 μm .) In each cell, the change in dry mass measurement is less than 1% of the initial measurement: 262.3 ± 1.0 pg (0.38%) in cell 1, 265.1 ± 1.9 pg (0.72%) in cell 2, and 246.1 ± 2.2 pg (0.89%) in cell 3.

areas represent the SD calculated by the propagation of errors method (10). We found the growth rate to be size-dependent for all three cell types. Together, results in Fig. 3 and 4 show that growth rates of proliferating lymphoblastoid and epithelial cells increase with cell mass and that the biomass of a dividing cell is distributed unevenly among daughters. These data are in accord with an exponential model of cell growth and imply the existence of an intrinsic mechanism that actively coordinates growth with division in epithelial cells.

Discussion

Cell growth, balanced by cell division, determines cell size, a fundamental parameter of cells. “Cell growth” is defined as an increment in biomass over time; however, size has a more complex definition. Geometric size [i.e., volume, length (in the case of symmetrical specimens)] is commonly used as a measure of size, and cell growth is typically expressed as volume increase over time. This preference for geometric volume is largely due to the convenience, accuracy, and availability of the Coulter counter, a readily available and accurate means of determining cell volume. Therefore, conclusions on the mechanism of cell size control are usually based on geometric size. Until recently, the best-supported conclusions have been in fission yeast, where “geometric size” appears to be sensed by intrinsic mechanisms in a way that coordinates cell growth with cell division (3, 4). Recent data showing exponential cell growth in suspension mammalian cells agree with this suggestion (7, 10).

Optical measurements of geometric size are relatively straightforward in symmetrical and rigid specimens, such as fission yeast, the most established models for size homeostasis research. Metazoan cells, particularly adherent ones, are generally amorphous and flexible, and are thus considerably more challenging for size measurements. At present, optical methods for volume measurement are inadequate for unambiguously deriving the growth curve of proliferating adherent cells. Confocal laser scanning microscopy (CLSM) can be used to map the cell border, but volume reconstruction using CLSM typically requires multilayer scanning and intensive illumination, putting the cells at a real risk of phototoxicity followed by abnormal growth, checkpoint arrest, and programmed cell death (46). In contrast, interferometry-based techniques use low-intensity transillumination and do not require any chemical staining or protein fluorescence labeling to measure the cell’s size or growth. Moreover, such methodology measures the cell’s biomass rather than volume or other mass surrogates.

Interferometric methods have been used for dry mass measurements for half a century, but it is only recently that these

methodologies have reached the accuracy required for studying cell growth. These improvements in accuracy were made by improving noise suppression by adopting a common path configuration (19), by using broadband light (8), or by adding up multiple phase images (47). In this paper, we demonstrated a new method that is not only low in noise but corrects diffraction artifacts. This newly developed method (SPM) is based on a unique 2D data mapping of the scattered fields recorded at multiple angles of illumination. SPM efficiently provides an accurate value of cell dry mass unaffected by diffraction artifacts, and thus can be used for both thick and thin cells. In addition, as evidenced by the trypsin experiment, it has an estimated measurement precision of 1% of the total mass and even higher estimated measurement sensitivity (2.5 fg). Furthermore, SPM provides about twice as high spatial resolution as single-shot phase imaging.

With this improved method, we measured the dry mass of newborn and mitotic cells, as well as the mass distribution of

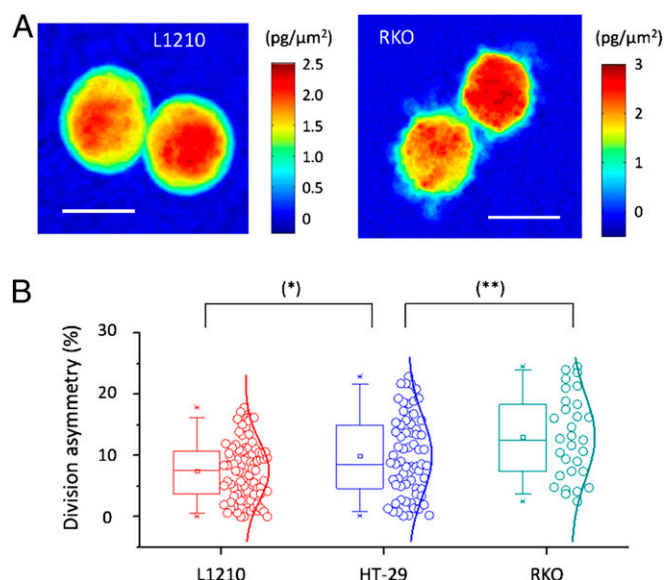


Fig. 3. Division asymmetry. (A) SPM images for the areal density of dry mass in dividing L1210 and RKO cells. (Scale bar, 10 μm .) (B) Division asymmetry of eukaryotic cells: $7.5 \pm 4.8\%$ in L1210 (red, 60 divisions), $10.0 \pm 6.4\%$ in HT-29 (blue, 70 divisions), and $13.0 \pm 6.8\%$ in RKO (green, 50 divisions) cells. * $P = 0.0077$; ** $P = 0.034$.

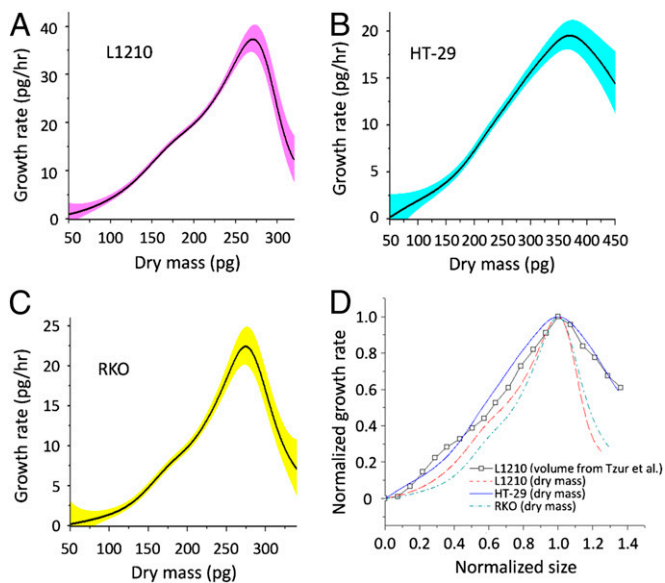


Fig. 4. Size dependency of cell growth. Average cell growth rate vs. cell dry mass calculated for L1210 (A), HT-29 (B), and RKO (C) cells using the Collins–Richmond conservation equation (details are provided in main text). (D) Three growth rate vs. cell dry mass curves (L1210, HT-29, and RKO cells) and one growth rate vs. cell volume curve [L1210 cells from the study by Tzur et al. (10)] were normalized by their own critical size and the maximum growth rate.

asynchronous cells growing naturally. Using these parameters and the Collins–Richmond conservation equation, we calculated the mass dependency of the growth rate for L1210 lymphoblasts and two epithelial cell types, HT-29 and RKO. For L1210 lymphoblasts, we showed a roughly linear relationship between the average growth rate and dry mass; however, this dependency is not completely uniform over the size range, and presumably over the cell cycle. For most of the size range, the growth rate increases with increasing mass in a steady-state population; however, beyond a critical size (cell mass = 275 pg), this trend is reversed and growth rate declines as a function of mass. In 80% of the cells, however, division occurs before the cells reach this mass (Fig. 4A). The overall relationship between dry mass and growth rate we found was almost identical to that previously reported using volume as a measure of size (10). In fact, if normalized for the maximum, the plots are nearly overlapping, as shown in Fig. 4D, suggesting that the density of nonaqueous materials in the cell remains constant in the population at 135.5 g/L. Because cell density seems constant in proliferating L1210 cells (17), these findings establish our technology as a high-resolution tool for size and growth measurements in living cells.

Our previous work on lymphoblastoid cells helped resolve a long-standing debate of whether mammalian cells follow a linear or exponential growth pattern (10), and therefore whether there is a feedback control maintaining cell size. However, cells grown in suspension may be exceptional. Conlon and Raff (5) raised this issue in their paper on linear growth in Schwann cells, writing “Our findings also do not exclude the possibility that animal cells such as lymphocytes, which can proliferate in suspension like yeast cells, might use cell-size checkpoints to coordinate their growth with cell-cycle progression.” Applying the SPM method described here to two epithelial cell lines, HT-29 and RKO, we show in both cases that these cell lines, like L1210 cells, maintain a linear relationship between the average growth rate and cell mass over the majority of the size range. The Collins–Richmond plots calculated for both cell types were remarkably similar to that

of L1210 (Fig. 4D) and demonstrate that the exponential growth model is not restricted to lymphoblastoid cells grown in suspension. In addition, we quantify with unprecedented accuracy the biomass distribution in daughter cells immediately after division. The average mass asymmetry was lowest in daughter L1210 cells (7.5%), recapitulating the 7% asymmetry estimated by volume (10). Biomass asymmetry was significantly greater in both epithelial cell lines, averaging $\geq 10\%$ in both cases. Perhaps physical stress caused by surrounding cells, the uneven microenvironment a dividing adherent cell experiences, and the surface itself introduce biophysical perturbations that increase asymmetry relative to cells that are dividing freely in suspension. Partitioning ribosomes, total proteins, carbohydrates, and lipids with over 10% asymmetry is significant. In a simple exponential model of growth, where size is the only parameter affecting growth rate, daughter cells that divide unevenly will grow at a different pace. Thus, without a size gate that feeds back on the timing of division, cell size distribution in steady-state populations cannot remain constant. Fig. S2 illustrates this point; for example, if cells divide with 10% asymmetry and daughter cells grow without the size gate up to twice their original mass, the relative difference between the largest and smallest cells in the population, starting from a single cell, will be 92% after nine cycles. Therefore, in at least two adherent cell lines of mammalian origin, similar to the situation for unattached lymphoblast cells, there must be a cell-autonomous size regulator that couples cell growth to the cell cycle.

These results differ from those of Conlon and Raff (5) on adherent Schwann cell cultures, where a size independence of growth was suggested. This might simply reflect differences in cell type or, alternatively, differences in experimental design. Interestingly, we found for all three cell types that large cells above a critical size (L1210: 271 pg, HT-29: 370 pg, and RKO: 275 pg) reverse their growth pattern. For all cell types, at least half of the cells (L1210: 80%, HT-29: 62%, and RKO: 56%) divide before reaching this critical size (Fig. S1 A, D, and G) (i.e., maintain a linear and monotonic relationship between mass and growth rate throughout their life cycle). For cells beyond this point, size seems to convey a slight growth inhibition. This growth limitation can be either “passive” (e.g., induced by biophysical properties like surface to volume ratio) or, alternatively, “active” (e.g., diluting a rate-limiting component below a critical value). In L1210 cells, the probability of cell division varies independently with cell size and cell age (10). It is therefore plausible that the growth of large cells is a bit delayed until “time” dominates and induces division. Such a mechanism can potentially limit cell size range in a steady-state population.

In summary, the approach we described here, along with others under development (7–10), enables the ability to measure growth in both suspension and attached cells under a wide variety of commonly studied conditions.

Materials and Methods

Microscope Setup. The SPM system was built based on an off-axis digital holography setup, which enables fast acquisition of phase images. For illumination, we used a collimated laser beam from a He-Ne laser ($\lambda = 633$ nm). The angle of illumination at the sample plane was varied using a double-axis galvanometer mirror (Cambridge Technology) that was installed at the conjugate plane to the sample plane. The high-N.A. condenser lens (1.4 N.A.; Nikon) and objective lens (1.4 N.A., UPLSAPO; Olympus) enabled the angular coverage of up to 60° with respect to the optical axis. The spiral path of the focused beam enabled fast scanning of the entire N.A., and a complementary metal-oxide semiconductor (CMOS) camera (1024PCI; Photron) captured 400 images within less than a second.

Data Analysis. A custom-built MATLAB (MathWorks) code was used to retrieve the scattered light fields, both amplitude and phase delay, from the raw interferogram images acquired with the CMOS camera (27). The phase images at varying incident angles were mapped in the 2D spatial frequency

plane using Eq. 1. The inverse Fourier transform of the 2D mapping (Eq. 2) provides the areal density of a sample, the integral of which provides cell dry mass. The cell boundary was detected with thresholding and manual selection. The probability density and cumulative density functions of dry mass for each group were obtained using a custom-built code for kernel density estimation.

Cell Culture and Sample Preparation. L1210 mouse lymphoblasts were grown in Leibovitz's L-15 CO₂ independent media (21083-027; Invitrogen) supplemented with 10% FBS (10438026; Invitrogen), 1 g/L D-(+)-glucose solution (G8270; Sigma-Aldrich), and 1% (vol/vol) 100× penicillin/streptomycin solution (15140-122; Invitrogen). Before each measurement set, L1210 cells from an exponentially growing population were cultured on a 40-mm coverslip precoated with poly-L-lysine (P8920; Sigma-Aldrich). HT-29 and RKO colon cancer cells were cultured in DMEM (21063-029; Invitrogen) supplemented with 10% FBS and 1% 100× penicillin/streptomycin solution. At 70–80% confluency, cells were passaged and seeded on a coverslip and then incubated for 24 h. Polystyrene beads (1 μm) were purchased from Polysciences, Inc. (64030-15).

On-Stage Cell Culture System. Cells were observed while grown in a temperature-controlled flow chamber (RC-31; Warner Instruments). The oxygen concentration and pH within the chamber were maintained by the continuous flow of conditioned media pre-equilibrated with air containing 5% CO₂.

The flow rate of the media was determined to guarantee that the rate of oxygen supply was twice as large as the rate of oxygen consumption by the cells inside the chamber. The flow speed inside the chamber was independently controlled by changing the thickness of a spacer, which defines the volume of the chamber. The flow speed was small enough not to disturb cell growth or division (shear stress at wall <1 mPa). A heater embedded in the chamber maintained the temperature of the entire system at 37 °C. Line heaters (MTC-HLS-1; Bioscience Tools) were wrapped around the condenser and objective lenses to minimize heat loss through the immersion oil that is in direct contact with the lenses.

ACKNOWLEDGMENTS. We thank Dr. Ana Hernandez for the RKO cells and Drs. Dan Fu and Ran Kafri for helpful discussions. This work was funded by Grant P41-RR02594-18 of the National Center for Research Resources of the National Institutes of Health (to Y.S., R.R.D., and Z.Y.), Grant DBI-0754339 of the National Science Foundation (to Y.S., R.R.D., and Z.Y.), the Hamamatsu Corporation (Y.S., R.R.D., Z.Y.), Marie Curie International Reintegration Grant PIRG-GA-2010-277062 (to A.T.), and the Israeli Centers of Research Excellence program [center no. 41/11 (A.T.)]. Y.S. was supported by a fellowship from the Kwanjeong Educational Foundation. The research conducted by Y.S. has been included in his PhD dissertation submitted to the Massachusetts Institute of Technology. Further support was provided by National Institute of General Medical Sciences Grant GM26875 (to M.W.K.).

1. Jorgensen P, Tyers M (2004) How cells coordinate growth and division. *Curr Biol* 14(23):R1014–R1027.
2. Edgar BA, Kim KJ (2009) Cell biology. Sizing up the cell. *Science* 325(5937):158–159.
3. Martin SG, Berthelot-Grosjean M (2009) Polar gradients of the DYRK-family kinase Pom1 couple cell length with the cell cycle. *Nature* 459(7248):852–856.
4. Moseley JB, Mayeux A, Paoletti A, Nurse P (2009) A spatial gradient coordinates cell size and mitotic entry in fission yeast. *Nature* 459(7248):857–860.
5. Conlon I, Raff M (2003) Differences in the way a mammalian cell and yeast cells coordinate cell growth and cell-cycle progression. *J Biol* 2(1):7.
6. Echave P, Conlon IJ, Lloyd AC (2007) Cell size regulation in mammalian cells. *Cell Cycle* 6(2):218–224.
7. Godin M, et al. (2010) Using buoyant mass to measure the growth of single cells. *Nat Methods* 7(5):387–390.
8. Mir M, et al. (2011) Optical measurement of cycle-dependent cell growth. *Proc Natl Acad Sci USA* 108(32):13124–13129.
9. Park K, et al. (2010) Measurement of adherent cell mass and growth. *Proc Natl Acad Sci USA* 107(48):20691–20696.
10. Tzur A, Kafri R, LeBleu VS, Lahav G, Kirschner MW (2009) Cell growth and size homeostasis in proliferating animal cells. *Science* 325(5937):167–171.
11. DeBlois RW, Bean CP (1970) Counting and sizing of submicron particles by resistive pulse technique. *Rev Sci Instrum* 41(7):909–916.
12. Elliott SG, McLaughlin CS (1978) Rate of macromolecular synthesis through the cell cycle of the yeast *Saccharomyces cerevisiae*. *Proc Natl Acad Sci USA* 75(9):4384–4388.
13. Killander D, Zetterberg A (1965) Quantitative cytochemical studies on interphase growth. I. Determination of DNA, RNA and mass content of age determined mouse fibroblasts in vitro and of intercellular variation in generation time. *Exp Cell Res* 38:272–284.
14. Zetterberg A, Killander D (1965) Quantitative cytochemical studies on interphase growth. II. Derivation of synthesis curves from the distribution of DNA, RNA and mass values of individual mouse fibroblasts in vitro. *Exp Cell Res* 39(1):22–32.
15. Di Talia S, Skotheim JM, Bean JM, Siggia ED, Cross FR (2007) The effects of molecular noise and size control on variability in the budding yeast cell cycle. *Nature* 448(7156):947–951.
16. Kubitschek HE (1968) Constancy of uptake during the cell cycle in *Escherichia coli*. *Biophys J* 8(12):1401–1412.
17. Loken MR, Kubitschek HE (1984) Constancy of cell buoyant density for cultured murine cells. *J Cell Physiol* 118(1):22–26.
18. Bryan AK, Goranov A, Amon A, Manalis SR (2010) Measurement of mass, density, and volume during the cell cycle of yeast. *Proc Natl Acad Sci USA* 107(3):999–1004.
19. Popescu G, et al. (2008) Optical imaging of cell mass and growth dynamics. *Am J Physiol Cell Physiol* 295(2):C538–C544.
20. Kak AC, Slaney M (1988) *Principles of Computerized Tomographic Imaging* (IEEE Press, New York).
21. Collins JF, Richmond MH (1962) Rate of growth of *Bacillus cereus* between divisions. *J Gen Microbiol* 28:15–33.
22. Donachie WD, Blakely GW (2003) Coupling the initiation of chromosome replication to cell size in *Escherichia coli*. *Curr Opin Microbiol* 6(2):146–150.
23. Dolznig H, Grebien F, Sauer T, Beug H, Müllner EW (2004) Evidence for a size-sensing mechanism in animal cells. *Nat Cell Biol* 6(9):899–905.
24. Liang J, Grimm B, Goelz S, Bille JF (1994) Objective measurement of wave aberrations of the human eye with the use of a Hartmann-Shack wave-front sensor. *J Opt Soc Am A Opt Image Sci Vis* 11(7):1949–1957.
25. Bon P, Maucort G, Wattellier B, Monneret S (2009) Quadriwave lateral shearing interferometry for quantitative phase microscopy of living cells. *Opt Express* 17(15):13080–13094.
26. Creath K (1988) Phase-measurement interferometry techniques. *Prog Optics* 26(26):349–393.
27. Ikeda T, Popescu G, Dasari RR, Feld MS (2005) Hilbert phase microscopy for investigating fast dynamics in transparent systems. *Opt Lett* 30(10):1165–1167.
28. Iwai H, et al. (2004) Quantitative phase imaging using actively stabilized phase-shifting low-coherence interferometry. *Opt Lett* 29(20):2399–2401.
29. Wang Z, et al. (2011) Spatial light interference microscopy (SLIM). *Opt Express* 19(2):1016–1026.
30. Reed Teague M (1983) Deterministic phase retrieval: A Green's function solution. *J Opt Soc Am A* 73(11):1434–1441.
31. Streibl N (1984) Phase imaging by the transport equation of intensity. *Opt Commun* 49(1):6–10.
32. Barer R (1952) Interference microscopy and mass determination. *Nature* 169(4296):366–367.
33. Barer R (1957) Refractometry and interferometry of living cells. *J Opt Soc Am* 47(6):545–556.
34. Barer R, Tkaczyk S (1954) Refractive index of concentrated protein solutions. *Nature* 173(4409):821–822.
35. Zhao H, Brown PH, Schuck P (2011) On the distribution of protein refractive index increments. *Biophys J* 100(9):2309–2317.
36. Wolf E (1969) Three-dimensional structure determination of semi-transparent objects from holographic data. *Opt Commun* 1(4):153–156.
37. Devaney AJ (1981) Inverse-scattering theory within the Rytov approximation. *Opt Lett* 6(8):374–376.
38. Sung Y, et al. (2009) Optical diffraction tomography for high resolution live cell imaging. *Opt Express* 17(1):266–277.
39. Paganin D, Nugent K (1998) Noninterferometric phase imaging with partially coherent light. *Phys Rev Lett* 80(12):2586–2589.
40. Kasarova SN, Sultanova NG, Ivanov CD, Nikolov ID (2007) Analysis of the dispersion of optical plastic materials. *Opt Mater (Amst)* 29:1481–1490.
41. Boucrot E, Kirchhausen T (2008) Mammalian cells change volume during mitosis. *PLoS ONE* 3(1):e1477.
42. Habela CW, Sontheimer H (2007) Cytoplasmic volume condensation is an integral part of mitosis. *Cell Cycle* 6(13):1613–1620.
43. Anderson EC, Bell GI, Petersen DF, Tobey RA (1969) Cell growth and division. IV. Determination of volume growth rate and division probability. *Biophys J* 9(2):246–263.
44. Parzen E (1962) On estimation of a probability density function and mode. *Ann Math Stat* 33(3):1065–1076.
45. Rosenblatt M (1956) Remarks on some nonparametric estimates of a density function. *Ann Math Stat* 27(3):832–837.
46. Hoebe RA, et al. (2007) Controlled light-exposure microscopy reduces photobleaching and phototoxicity in fluorescence live-cell imaging. *Nat Biotechnol* 25(2):249–253.
47. Kim M, et al. (2011) High-speed synthetic aperture microscopy for live cell imaging. *Opt Lett* 36(2):148–150.